Forest above ground biomass estimation methodology based on polarization coherence tomography

LUO Huanmin[1], CHEN Erxue[2], LI Zengyuan[2], CAO Chunxiang[3]

1. *Institute of Geo-Spatial Information Science and Technology*, *University of Electronic Science and Technology of China*, *Sichuan Chengdu* 610054, *China*;
2. *Institute of Forest Resources Information Technique of Chinese Academy of Forestry*, *Beijing* 100091, *China*;
3. *State Key Laboratory of Remote Sensing Science*, *Jointly Sponsored by the Institute of Remote Sensing Applications of Chinese Academy of Sciences and Beijing Normal University*, *Beijing* 100101, *China*

Abstract: Forest above ground biomass (AGB) estimation using microwave backscattering coefficient is normally limited to low level AGB because of the "saturation" problem in backscattering coefficient. In addition, forest height may be used to estimate AGB by allometric equation, but the changing conditions of the forest in terms of density, tree species composition *etc*. limit the accuracy and performance of the method. In order to overcome the above disadvantages and improve the estimation accuracy, a method for AGB estimation is proposed in this paper, which is based on polarization coherence tomography (PCT) technology. Using repeat pass ESAR L-band PolInSAR data collected by DLR at the Traunstein test site, the radar relative reflectivity function of each pixel is reconstructed using PCT, from which the average relative reflectivity profiles for the 20 validation stands are computed. Then 9 profile characteristic parameters closely related to biomass are defined and extracted for each forest stand. The natural logarithms of these 9 profile parameters are taken as independent variables for multivariate linear regression analysis with the natural logarithm of the field-measured AGB as dependent variable using stepwise regression method. Forest AGB estimation model is established and evaluated, and the factors possibly affecting the performance of the AGB estimation model are also analyzed. The results show that these parameters, which are extracted from the average relative reflectivity function inversed with PCT, are sensitive to forest AGB. The accuracy of AGB estimation can be improved if we make full use of the information contained in the relative reflectivity function.

Key words: polorimetric interferometric SAR, polarization coherence tomography, stepwise regression analysis method, forest above ground biomass

CLC number: TN957.51 **Document code:** A

Citation format: Luo H M, Chen E X, Li Z Y and Cao C X. 2011. Forest above ground biomass estimation methodology based on polarization coherence tomography. *Journal of Remote Sensing*, **15**(6): 1138–1155

1 INTRODUCTION

Large scale forest above ground biomass (AGB) mapping with high accuracy is of great significance for global carbon cycle and climate change research. Many scholars have carried out forest biomass estimation research by remote sensing technology (Chen, 1999; Yang, *et al*., 2005; Xu, *et al*., 2008; Lu, *et al*., 2006). One commonly used method is based on empirical or semi-empirical models fitted between radar backscatter power or optical reflectance and field-measured biomass. However, when biomass level is high, the signal "saturation" phenomenon will occur (Dobson, *et al*., 1995; Ranson, *et al*., 1997; Steininger, 2000; Wang, *et al*., 2006). In recent years polarimetric interferometric SAR (PolInSAR) and LiDAR technology have been developed rapidly. Tree height extracted from PolInSAR or LiDAR data can be converted to AGB by tree height to biomass allometric equations. The method solves, to some extent, the signal saturated problem (Mette, 2007)[112,121], but the changing conditions of the forest in terms of density, tree species composition *etc*. limit the accuracy and performance of the method due to their close relationships with AGB. Therefore, we can speculate that the forest AGB estimation accuracy should be further improved if the stand vertical structure information is con-

Received: 2010-11-08; **Accepted:** 2011-01-30

Foundation: The National Basic Research Program (973 Program) (No. 2007CB714404); The National Natural Science Foundation of China (No. 60890074)

First author biography: LUO Huanmin (1972—), male, Ph. D. candidate. He received master degree of measurement technology and instruments from University of Electronic Science and Technology of China in 2005, mainly research on the polarimetric and interferometric SAR remote sensing, has published six papers. E-mail: Lhm123345@qq.com

Corresponding author biography: CHEN Erxue (1968—), male, professor, received the Ph. D. degree from the Chinese Academy of Forestry, Beijing, China, in 2004. His main research interests include the theories and applications of radar remote sensing. He has published more than 10 papers about radar remote sensing applications during these five years. E-mail: chenerx@caf.ac.cn

sidered comprehensively in the AGB estimation model.

However, we know that for forest vertical structure information, there are always different descriptions and ground-based observation methods from different scholars and research fields (such as forest management, forest ecology, *etc*.). The parameter M , which is used to describe forest vertical structure information has a common characteristic, namely M changes with height denoted by z and can be abstracted as a function $M(z)$. If $M(z)$ can be accurately measured, forest volume (V), AGB and other parameters representing integrated structure of forest should be accurately estimated. With the advanced remote sensing techniques such as LiDAR and PolInSAR, the vertical distribution of a certain physical parameter, denoted as $E(z)$, can be inversed. However, $E(z)$ is not equivalent to $M(z)$. Only by establishing the relationship between $E(z)$ and $M(z)$ or V, AGB, can thematic information of interest to the user such as $M(z)$, V, AGB, and so on be obtained.

Relative reflectivity function $f(z)$ based on SAR data is a specific form of $E(z)$ as described above. There are two classes of methods in the literatures for inversing $f(z)$. One class is proposed by Treuhaft, *et al*. (2009a, 2009b) which uses C-band multi-baseline InSAR data to estimate $f(z)$. The method is based on invertible coherent scattering model containing the vertical structure function. Profile is estimated by adjusting structure parameters until the difference between vectors of InSAR coherence and phase measured by multi-baseline InSAR observation with different flying height and the corresponding vectors of model estimated coherence and phase is minimum. The other is suggested by Cloude (2006) that uses PolinSAR data to estimate $f(z)$ by polarization coherence tomography technology. Based on the dependence of coherence on vertical structure variations in forest scene, PCT can be used to estimate arbitrary vertical profile via a Fourier-Legendre series expansion of the unknown vertical profile followed by the estimation of the parameters of this series from interferometric coherence data for each pixel. However, this approach is different from the first method in assuming that $f(z)$ is of Gaussian distribution function.

In case of the estimation of $M(z)$ and AGB from $f(z)$ derived by the C-band multi-baseline InSAR, Treuhaft, *et al*. (2002, 2003) combined $f(z)$ from InSAR data and LAI from hyperspectral data to estimate the forest leaf area density (LAD) which is the vertical distribution of LAI and similar to $M(z)$ described previously. LAD was compared with the ground measured value and a good agreement was found. Treuhaft (2003) further applied LAD to estimate the AGB, and achieved good results. Although Cloude (2006) already pointed out that $f(z)$ inversed by PCT had great potential in AGB estimation, and was supported by later studies (Cloude & Papathanassiou, 2008; Praks, *et al*., 2008; Chen, *et al*., 2009; Luo, *et al*., 2010). At present there is still a lack of researches applying it to forest AGB estimation. Therefore, here we investigate the potential and limitations of forest relative reflectivity function for forest AGB estimation using PCT from forest inventory data of 20 forest stands and corresponding repeat pass ESAR L-band PolInSAR data collected by DLR at the Traunstein test site.

2 TEST SITE AND DATA SETS

The test site is located near the Traunstein in southern German and mainly is covered by agricultural fields, pasture, forests and some urban areas in the western area. The topography is flat with elevation varying from 600 to 650 m. The dominant tree species of this site are composed of spruce, beech and fir. On October 11, 2003, repeat pass L-band airborne PolInSAR data covering the site was obtained onboard DLR ESAR sensor. The flight altitude was 3000 m above the ground; the nominal spatial baseline was 5 m and the temporal baseline was 20 min. The incidence angle increased from 25° in near range to 60° in far range. The data were processed for 1.5 m range resolution and 3.0 m resolution in azimuth. Master and slave images were provided as coregistered InSAR pairs. The plat earth phase image and the effective wave number image were also provided. The polarization color composite image is shown in Fig. 1. The color scheme is based on the Pauli vector by assigning |HH-VV|, |HV|, and |HH+VV| as Red, Green and Blue channel, respectively. It can be seen that the forests possess a comparably strong cross-polarization response (volume scattering) and significant double bounce (|HH-VV|) can only be noted over parts of the city of Traunstein. The red line shown in Fig. 1 is along the azimuth direction from top to bottom. The detailed forest inventory data for the 20 validation stands as shown in Fig. 1 were collected. The mean dominant heights of forest stand, denoted as h_{100} (the mean height of the 100 highest trees per hectare) of 20 validation stands were estimated from the inventory data. Then the AGB of each forest stands was calculated by height to biomass allometric equation and taken as ground measured forest stand average AGB (Mette, 2007)[35, 36]. The AGB of the forest stands ranges from 38.7 t / hm^2 to 445.2 t / hm^2.

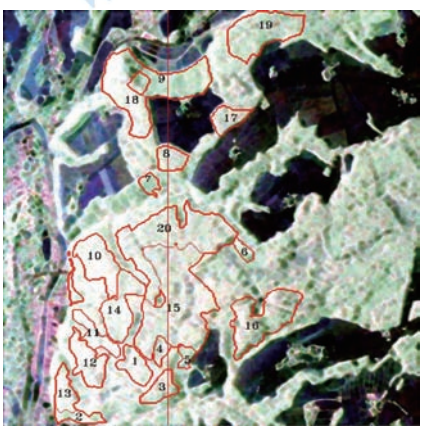

Fig. 1 RGB composite image of the polarimetric SAR data of the Traunstein scene in the Pauli basis

3 PRINCIPLES AND METHODS

3.1 Reconstruction of the vertical structure function by PCT

Cloude (2006)[7-25] discussed the PCT algorithm in detai with the main processes described as below. The complex interferometric coherence for the two complex signals $\boldsymbol{s}_1$ and $\boldsymbol{s}_2$ which are collected at ends 1 and 2 of a spatial baseline of InSAR system can be formulated as follows:

$$\tilde{\gamma}_w = \frac{\left\langle \boldsymbol{s}_1 \boldsymbol{s}_2^* \right\rangle}{\sqrt{\left\langle \boldsymbol{s}_1 \boldsymbol{s}_1^* \right\rangle \left\langle \boldsymbol{s}_2 \boldsymbol{s}_2^* \right\rangle}} = \mathrm{e}^{i\phi_0} \frac{\int_0^{h_v} f(\boldsymbol{w}, z) \mathrm{e}^{ik_z z} \mathrm{d}z}{\int_0^{h_v} f(\boldsymbol{w}, z) \mathrm{d}z}$$

$$0 \leqslant |\tilde{\gamma}| \leqslant 1 \tag{1}$$

where ϕ_0 is the ground topography phase, $k_z = \frac{4\pi\Delta\theta}{\lambda \sin\theta}$ is the effective wave number, θ is the incidence angle $\Delta\theta$ is the apparent angular separation of the baseline from the scattering point, λ is the SAR wavelength in free space, h_v is the average tree height within a pixel and referred to as the tree height in the following text, $f(\boldsymbol{w}, z)$ that changs with height z is the radar relative reflectivity function in a certain polarization state $\boldsymbol{w}$. The minimum value of z is 0, corresponding to the position of the bottom of the vegetation layer. The maximum value of z is h_v. By applying the PCT algorithm to PolInSAR data, the $f(\boldsymbol{w}, z)$ can be estimated from Eq. (2)

$$\hat{f}_{L2}(\boldsymbol{w}, z) = \frac{1}{\hat{h}_v}\Big(1 - \hat{a}_{10}(\boldsymbol{w}) + \hat{a}_{20}(\boldsymbol{w}) + \frac{2z}{\hat{h}_v}(\hat{a}_{10}(\boldsymbol{w}) - 3\hat{a}_{20}(\boldsymbol{w})) + \hat{a}_{20}(\boldsymbol{w})\frac{6z^2}{\hat{h}_v^2}\Big) \tag{2}$$

where $0 \leqslant z \leqslant \hat{h}_v$, $\hat{f}_{L2}(\boldsymbol{w}, z)$ is the second-order approximation of Legendre series of $f(\boldsymbol{w}, z)$, For easy description, the subscript will be omitted in the following text. $\hat{h}_v$ is the estimation of h_v. The Legendre polynomial coefficients $\hat{a}_{10}(\boldsymbol{w})$ and $\hat{a}_{20}(\boldsymbol{w})$ can be calculated from Eq. (3).

$$\hat{a}_{10}(\boldsymbol{w}) = \frac{\mathrm{Im}(\tilde{\gamma}_k)}{f_1}$$

$$\hat{a}_{20}(\boldsymbol{w}) = \frac{\mathrm{Re}(\tilde{\gamma}_k)}{f_2} - \frac{f_0}{f_2}$$

$$\tilde{\gamma}_k = \tilde{\gamma}(\boldsymbol{w})\mathrm{e}^{-i(\hat{k}_v + \hat{\phi}_0)}$$

$$k_v = \frac{k_z \hat{h}_v}{2} \quad f_0 = \frac{\sin k_v}{k_v} \quad f_1 = i\Big(\frac{\sin k_v}{k_v^2} - \frac{\cos k_v}{k_v}\Big)$$

$$f_2 = \frac{3\cos k_v}{k_v^2} - \Big(\frac{6 - 3k_v^2}{2k_v^3} + \frac{1}{2k_v}\Big)\sin k_v \tag{3}$$

It can be seen that as long as the tree height $\hat{h}_v$ and the ground topography phase $\hat{\phi}_0$ are estimated, and the complex coherence $\tilde{\gamma}(\boldsymbol{w})$ for the polarization state $\boldsymbol{w}$ is calculated, k_v and $\tilde{\gamma}_k$ can be gotten. Then The Legendre polynomial coefficients $\hat{a}_{10}(\boldsymbol{w})$ and $\hat{a}_{20}(\boldsymbol{w})$ can be obtained. Thus the relative reflectance function $\hat{f}(\boldsymbol{w}, z)$ of each pixel in the corresponding polarization state can be reconstructed from Eq. (2).

We can see from the above description that the tree height and the ground topography phase are the two key input parameters for the reconstruction of radar relative reflectivity function. The estimation errors of them have direct impacts on the estimation accuracy of the relative reflectivity function. There are many ways (Cloude & Papathanassiou, 2003; Bai, *et al*., 2010) to extract the tree height from PolInSAR data. For L-band PolInSAR data of the Traunstein test site, the difference of complex coherence phases between polarization channels is small and there is non-volumetric related decorrelation in complex coherence. So in the process of estimation of tree height, if coherence phase information alone is used it will lead to underestimation, while if coherence amplitude information alone is used it will lead to overestimation. In order to improve the accuracy of tree height estimation, in this paper a hybrid inversion method based on fusion of the coherence amplitude and phase information is used, which combines interferometric coherence optimization and compensation of non-volumetric scattering decorrelation (Luo, *et al*., 2010). After the process of co-registration, filtering, flat earth phase removal and multi-look operation, the phase diversity (PD) interferometric coherence optimization method (Tabb, *et al*., 2002) was used to obtain the coherences $\tilde{\gamma}(\boldsymbol{w}_v)$ and $\tilde{\gamma}(\boldsymbol{w}_s)$ in polarization channels dominated by volume and surface scattering, respectively. Then we can find that the ground phase (Cloude, 2006) and estimate tree height by hybrid inversion method based on fusion of the coherence amplitude and phase information (Luo, *et al*., 2010)[818-820]. The inversed tree heights of all the pixels in each forest stand, whose boundary is shown as the red polygons in Fig. 1, are arithmetic averaged as the estimated forest stand heights. The estimated heights are plotted against ground measured forest stand average heights in Fig. 2. The coefficient of determination (R^2) is up to 0.8630 with the average error of 0.90 m and RMSE of 3.11 m.

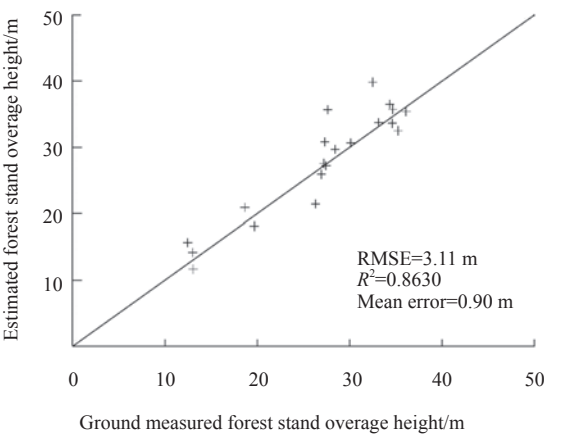

Fig. 2 Scatter diagram of ground measured average forest stand height with that estimated by the phase and amplitude hybrid inversion method based on interferometric coherence optimization and non-volumetric decorrelation compensation

The relative reflectivity function $\hat{f}(\boldsymbol{w}, z)$ of each pixel in the area covered by forest is obtained from PCT in polarization channel dominated by volume scattering. Fig. 3 shows the $\hat{f}(\boldsymbol{w}, z)$ sliced along the red line shown in Fig. 1, on which the horizontal direction represents pixel along the red line, the vertical one represents vertical height and the color reflects the relative reflectivity of radar backscattering. Here we constrain color mapping only for the pix-

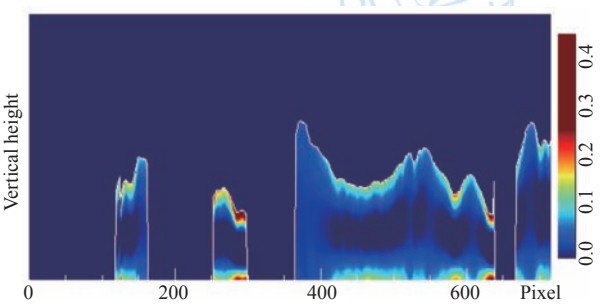

Fig. 3 Vertical profile of the relative reflectivity function from PCT in the SAR azimuth direction (along the red line in Fig. 1)

els whose $\hat{f}(\boldsymbol{w}, z)$ value ranges from 0 to 0.25, and the pixels with value exceed 0.25 are represented by the color of value 0.25. We can see that the relative reflectivity contributed by the volume scattering from the upper part of forest decays with the increasing of depth. However, there is relative strong reflectivity contributed by volume scattering in the forest near the ground surface. This indicates that there may be an underlying dense shrub layer.

3.2 Calculation forest stand average relative reflectance function and the definition of characteristic parameters

The $\hat{f}(\boldsymbol{w}, z)$ from Eq. (2) is calculated on the pixel scale, while ground measured forest AGB is provided by average ABG on stand scale. Therefore, it needs to calculate the average $\hat{f}(\boldsymbol{w}, z)$ on stand scale. Boundaries of the 20 inventory stands are drawn as the red polygons in Fig. 1. $\hat{f}(\boldsymbol{w}, z)$ of all the pixels in a stand is taken the arithmetic average as average $\hat{f}(\boldsymbol{w}, z)$ of the stand. So there is an average $\hat{f}(\boldsymbol{w}, z)$ for each of the stands, which is used in the following sections.

Fig. 4 shows the $\hat{f}(\boldsymbol{w}, z)$ of three forest stands of distinct AGB levels, namely low (AGB of No.14: 135.7 t/hm^2), medium (AGB of No.9: 303.3 t/hm^2) and high (AGB of No.20: 402.6 t/hm^2). In Fig. 4, h_2 and h_4 are the height positions where relative reflectivities are the closest to 0.0002 in the upper half of the $\hat{f}(\boldsymbol{w}, z)$ curve. These data between h_2 and h_4 constitute the first envelope. h_3 is the height position where relative reflectivity is the maximum in the first envelope. h_1 is the height position which is the first inflection point between the relative reflectivity corresponding to h_2 and the maximum relative reflectivity in the lower half of $\hat{f}(\boldsymbol{w}, z)$ curve. These data between the h_2 and the 0 height positions constitute the second envelope. We can see that the shape and peak position of the first envelope is closely related with the AGB. For the stand of high AGB, such as No.20, the peak is small, the span of the envelope (namely h_4–h_2) is larger, h_3 is high and the peak of the second envelope is smaller than that of the low AGB stand such as No.14. Through fitting the upper half of $\hat{f}(\boldsymbol{w}, z)$ curve by Gaussian function as the red dotted line in Fig. 4, we find that the Gaussian function can well fit the upper part of the $\hat{f}(\boldsymbol{w}, z)$ curve, indicating that the upper part of average relative reflectance function in stand scale is of Gaussian distribution. In order to analyze quantitatively the relationship between forest AGB and $\hat{f}(\boldsymbol{w}, z)$, we define 9 parameters to describe the characteristics of $\hat{f}(\boldsymbol{w}, z)$ as follows:

Parameter 1: $P_1=(h_4-h_2)/\hat{f}(\boldsymbol{w}, h_3)$

Parameter 2: $P_2 = \sum_{z=h_2}^{z=h_4} z \cdot \hat{f}(\boldsymbol{w}, z)$

Parameter 3, 4, 5: Through fitting the upper half curve by Gaussian function, we can get the three parameters P_3, P_4 and P_5 respectively. Parameter 3 is the reciprocal of height of the Gaussian. Parameter 4 is the center of the Gaussian. Parameter 5 is the width (the standard deviation) of the Gaussian.

Parameter 6, 7: $P_6 = 1/\sum_{z=h_2}^{z=h_3} \hat{f}(\boldsymbol{w}, z) \quad P_7 = 1/\sum_{z=0}^{z=h_1} \hat{f}(\boldsymbol{w}, z)$

Parameter 8: $P_8=P_6/P_7$

Parameter 9: $P_9 = \sum_{z=h_2}^{z=h_3} \hat{f}(\boldsymbol{w}, z) / \sum_{z=h_3}^{z=h_4} \hat{f}(\boldsymbol{w}, z)$

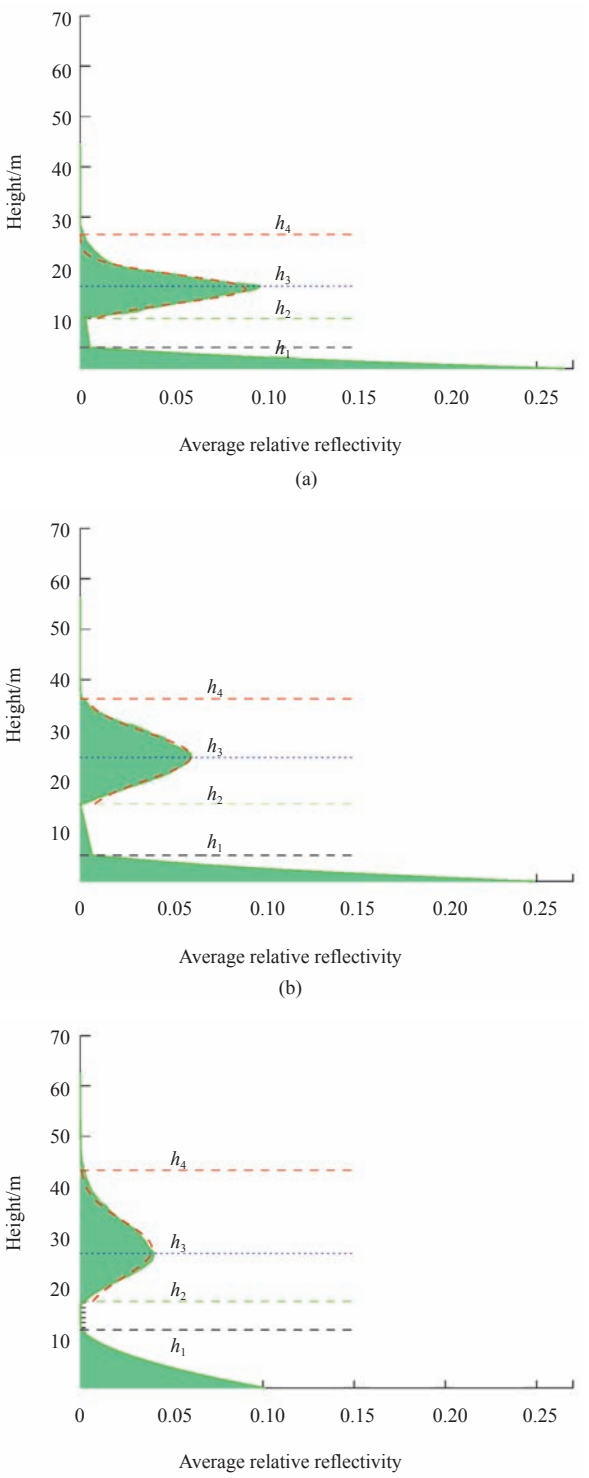

Fig. 4 Average relative reflectivity function in optimum polarization channel dominated by volume scattering of 3 typical forest stands in distinct AGB levels
(a) No. 14; (b) No. 9; (c) No. 20

3.3 Estimation model of forest AGB

Studies have shown that high correlation can be obtained by using the power function as shown by Eq. (4) to describe the relationship between the AGB and remote sensing observations by SAR

(Feng & Liu, 2005). So Eq. (4) is also used as the estimation model of forest AGB in this paper.

$$B = b_0' \prod_{i=1}^{n} P_i^{b_i} \tag{4}$$

where B is the AGB, P_i are the characteristic parameters extracted from $\hat{f}(\boldsymbol{w}, z)$, b_i and b_0' are the parameters of model, n is the number of characteristic parameters used in the model. In this paper, 9 parameters are defined to describe the characteristics of $\hat{f}(\boldsymbol{w}, z)$. So the maximum value for n is 9. Then we take natural logarithm of Eq. (4) as follows:

$$\ln(B)=\ln(b_0')+b_1\ln(P_1)+b_2\ln(P_2)+\cdots+b_n\ln(P_n) \tag{5}$$

We set

$$Y=\ln(B),\ b_0=\ln(b_0'),$$
$$X_1=\ln(P_1),\ X_2=\ln(P_2),\ \cdots,\ X_n=\ln(P_n)$$

Then we get the linear multivariate equation as follows:

$$Y=b_0+b_1X_1+b_2X_2+\cdots+b_nX_n \tag{6}$$

3.4 Construction and evaluation of AGB estimation model

In order to select significant characteristic parameters P_i (as independent variables) and find the best combination to predict the dependent variable (*i.e.*, AGB), we use multiple linear stepwise regression analysis method to construct AGB estimation model as shown by Eq. (6). The method allows independent variable to enter into the regression equation from less to more one by one (Gao, 2005). At each step, the independent variable not in the equation but with probability of the smallest F is entered, indicating the probability is sufficiently small. Variables already in the regression equation are removed if their probability of F becomes sufficiently large. The method terminates when no more variables are eligible for inclusion or removal. Finally, the variables retained have larger contribution to the dependent variable estimation and are significant variables. Variables excluded are variables whose ability to explain the variance in the dependent variable is weak.

In stepwise regression analysis, serious collinearity must be avoided since the severe collinearity between the variables will make regression model meaningless. Generally, collinearity can be indicated by tolerance or the variance inflation factor (VIF). Tolerance of an independent variable is denoted by the proportion of the variation not explained by the other variables to the variation of the dependent variable explained by the independent variable. It is calculated as $(1-R^2)$ where R^2 is the multiple correlation coefficient for the independent variable against all of the other variables in the regression equations. The VIF is the reciprocal of tolerance and low VIF indicates high degree of collinearity.

In addition, the consistency and significant of regression model is indicated by the squared correlation coefficient (R^2) and F statistics or P values, respectively. F is calculated as the regression mean square divided by the residual mean square. Then the P value can be obtained through F value table, which is used to determine significance of the regression equation at a given level.

3.5 The accuracy evaluation of AGB estimation model

The m-fold cross validation is used to assess the performance of the AGB estimation model established by the stepwise regression method. Namely the N samples are partitioned equally into m subsamples denoted respectively by G_1, G_2, G_3,…, G_m. Of the m subsamples, a single subsample G_v is retained as the validation data for testing the model, and the remaining $m-1$ subsamples G_t are used as training data. The cross-validation process is then repeated m times (the folds), with each of the m subsamples used exactly once as the validation data. The N results from the folds then can be used to calculate R^2 and RMSE with the measured values as the performance indicators of the AGB estimation model. The total number of validation stands is 20, so N is 20 and m is set to 10.

4 RESULTS AND ANALYSIS

4.1 Construction and analysis of AGB estimation model

In polarization channel $\boldsymbol{w}_v$ dominated by volume scattering, we obtain the average $\hat{f}(\boldsymbol{w}, z)$ for each of validation stands by the method as described in section 3.1. Then 9 characteristic parameters extracted from the $\hat{f}(\boldsymbol{w}, z)$ are used to do correlation analysis with the ground measured AGB of validation stands and the correlation coefficients R calculated are shown in Table 1. It can be seen that these parameters are to some extent related with biomass, of which the three parameters (P_3, P_4, P_5) from Gaussian fitting is of the highest correlation.

The 9 parameters are further used to carry the stepwise regression analysis with ground measured AGB. Based on probability of statistic F, namely P value, the independent variables which have P value of the largest F is entered, if that P value is less than or equal to 0.05. Variable already in the regression equation which has P value of the smallest F is removed if its P value is greater than or equal to 0.051. Finally, the three independent variables are selected, namely P_4, P_8 and P_9. The corresponding regression results are shown by model 1(M1) in Table 2. For each of independent variables in the M1, the tolerance is large (greater than 0.5) and VIF is small (less than 2), indicating that there is not collinearity problem in the three independent variables. F equals 95.9768 and P is 0.0000, showing that the regression models are significant. Based on the parameters estimated in M1, AGB regression equation can be constructed as follows:

$$\ln B=-2.9966+1.7806\ln(P_4)+$$
$$0.5765\ln(P_8)-0.2927\ln(P_9) \tag{7}$$

Table 1 Correlation coefficients between the 9 characteristic parameters and AGB using three different processing methods

Method \ Parameter	P_1	P_2	P_3	P_4	P_5	P_6	P_7	P_8	P_9
Method 1	0.8698	0.7041	0.9136	0.9355	0.8886	0.7627	0.7583	0.6487	0.2414
Method 2	0.8668	0.7486	0.9196	0.9402	0.8928	0.7828	0.7952	0.6659	0.2743
Method 3	0.8426	0.7229	0.8800	0.9281	0.8086	0.4783	0.6513	0.3255	0.5747

Note: Method 1: With non-volumetric decorrelation compensation in polarization channel dominated by volume scattering
Method 2: With non-volumetric decorrelation compensation in polarization channel dominated by surface scattering
Method 3: Without non-volumetric decorrelation compensation in polarization channel dominated by volume scattering

Table 2 Comparison of results of stepwise regression analysis for AGB estimation

Model	Model parameter	R^2	Adjusted R^2 (R_1^2)	Estimation parameter	F	P	Collinearity statistic	
							tolerance	VIF
M1	P_4 P_8 P_9	0.9474	0.9375	b_0=−2.9966 b_4=1.7806 b_8=0.5765 b_9=−0.2927	95.9768	0.0000	0.5453 0.6876 0.7067	1.8340 1.4544 1.4149
M2	P_4 P_8 P_7	0.9479	0.9381	b_0=−0.7766 b_4=1.8960 b_8=2.3706 b_7=−2.1366	97.0290	0.0000	0.3153 0.2053 0.1121	3.1715 4.8714 8.9168
MM2	P_4 P_8	0.9287	0.9203	b_0=−1.3218 b_4=1.5424 b_8=1.1565	110.7269	0.0000	0.7337 0.7337	1.3629 1.3629
M3	P_4 P_7	0.8932	0.8806	b_0=−4.8165 b_4=1.9590 b_7=0.8827	71.0603	0.0000	0.7081 0.7081	1.4122 1.4122
M4	$\hat{h}_v$	0.9031	0.8977	b_0=−0.5270 b_1=1.8457	167.7714	0.0000	1	1

Note: Model parameters are accurated to 4 digits after the decimal point

M1: This model is constructed from 9 characteristic parameters by stepwise regression method in polarization channel dominated by volume scattering

M2: This model is constructed from 9 characteristic parameters by stepwise regression method in polarization channel dominated by surface scattering

MM2: This model is M2 modified by excluding parameter P7

M3: This model is constructed from 9 characteristic parameters by stepwise regression method in polarization channel dominated by volume scattering without regard to the non-volumetric decorrelation factor in the process of estimation of forest stand height

M4: This model is constructed only from forest stand height inversed from coherence amplitude and phase information using stepwise regression method

The average AGB (natural logarithm) of the 20 forest stands estimated from Eq. (7) are plotted against the corresponding ground measured AGB (natural logarithm) as shown in Fig. 5. We can see that the RMSE is 0.15 t/hm^2, most of the points fall in the 1:1 line and a small part uniformly distribute on both sides of the line. The squared correlation coefficient is up to 0.9474. After eliminating the effects of the number of independent variables and the sample size on R^2, the square of the adjusted correlation coefficient R_1^2 can be obtained with value of 0.9375. This shows that there is a good correlation between the dependent variable and the 3 independent variables.

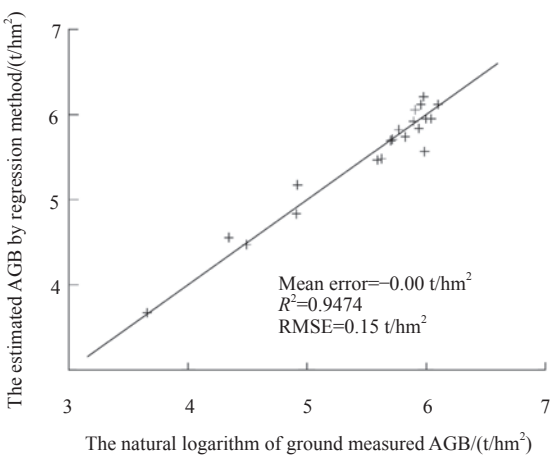

Fig. 5 Scatter diagram of ground measured forest stand AGB (natural logarithm) with estimated forest stand AGB (natural logarithm) by stepwise regression method

In addition, we can see from the sign of the estimated equation parameters P_4 and P_8 that the P_4 and P_8 have positive impact on estimation of AGB, namely the greater their values the greater the estimated AGB are. However, P_9 is just the opposite. This is consistent with that shown in Fig. 4.

4.2 Analysis of some factors affecting the performance of the AGB estimation model

The $\hat{f}(\boldsymbol{w}, z)$ estimated by PCT is closely related with polarization and is different in different polarization states. In addition, tree height and ground phase are the two key input parameters of PCT and their estimation errors directly affect the reconstruction accuracy of $\hat{f}(\boldsymbol{w}, z)$. Effects of the two factors on AGB estimation model will be analyzed below.

4.2.1 Effects of polarization on AGB estimation model

The $\hat{f}(\boldsymbol{w}, z)$ represents the relative reflectance function corresponding to a specific polarization ($\boldsymbol{w}$). In the process of reconstruction of $\hat{f}(\boldsymbol{w}, z)$ by the method described in section 3.1, if coherence $\tilde{\gamma}(\boldsymbol{w}_s)$, which corresponds to the polarization channel $\boldsymbol{w}_s$ dominated by surface scattering obtained by the PD interferometric coherence optimization method, is selected to calculate $\tilde{\gamma}_k$ using Eq. (3), we can obtain the relative reflectance function of each pixel which corresponds to the specific polarization channel $\boldsymbol{w}_s$. Nine stand characteristic parameters are further extracted to conduct correlation analysis with ground measured AGB. The results are shown in Table 1. Compared to the results corresponding to the polarization channel $\boldsymbol{w}_v$ dominated by volume scattering (row 1 in table 1), the correlation coefficient of each parameter changes little. The three independent variables P_4, P_7 and P_8 are selected by the stepwise regression method to construct model denoted by model 2 (M2), as shown in Table 2. Compared with M1, parameters P_4 and P_8 are retained and P_9 is replaced by P_7. This indicates that the characteristic parameter from the lower half of the $\hat{f}(\boldsymbol{w}, z)$ curve is sensitive in the polarization channel dominated by surface scattering, while this is just the opposite in the polarization channel dominated by volume scattering. However, the three parameters in the M2 have

very low tolerance, particularly the tolerance of P_7 is only 0.1121, indicating that there are serious collinearity among the three parameters. We further analyzed the correlation in the three parameters and find that the correlation coefficient between parameters P_7 and P_8 is up to 0.8487. After parameter P_7 is excluded, multiple linear stepwise regression analysis is used to construct model denoted by the modified model 2 (MM2) as shown in Table 2. We can see that there is no collinearity problem and the regression equation is significant. However, compared with M1, R^2 of MM2 decreases from 0.9474 to 0.9287. The above analysis shows that the polarization state dominated by volume scattering is more reasonable in forest AGB estimation in general.

4.2.2 Effects of inversion errors of tree height on AGB estimation model

First of all, tree height $\hat{h}_v$ of each pixel must be known in order to inverse $\hat{f}(\boldsymbol{w}, z)$ by PCT algorithm. There are many methods used to inverse directly $\hat{h}_v$ from PolInSAR data. In the process of tree height estimation, the non-volumetric scattering decorrelation factor (R_d) is not considered and the corresponding estimated forest stand average heights for 20 validation stands are plotted against ground measured forest stand average heights in Fig. 6. The average error is 2.71 m, with RMSE of 4.00 m and overestimation. These overestimated tree heights are taken as inputs of the PCT algorithm to reconstruct $\hat{f}(\boldsymbol{w}, z)$ for each of forest stands in the polarization state dominated by volume scattering. Then the 9 parameters, which are extracted from $\hat{f}(\boldsymbol{w}, z)$, are used to conduct correlation analysis with the ground measured AGB. The corresponding results are shown in line 3 of Table 1. It can be seen that the correlation coefficients of each of the parameters decrease slightly. These parameters are used to perform stepwise regression analysis with ground measured AGB and the corresponding results are shown as model 3 (M3) in Table 2. Parameters P_4 and P_7 are selected as the significant parameters for AGB estimation, indicating that parameters P_8 and P_9 describing characteristics of the upper part of the relative reflectivity function curve become less sensitive to the AGB, while the parameter P_7 describing characteristics of the lower part of the relative reflectivity function curve becomes more sensitive to the AGB because of the tree height estimation error. The value of F is 71.0603 and that of P is 0.0000, which indicates the regression equation is significant. However, compared with M1, R^2 is decreased from 0.9474 to 0.8932. These results indicate that the estimation errors of tree heights will be transmitted to the $\hat{f}(\boldsymbol{w}, z)$, thus reduce the accuracy of AGB estimation based on $\hat{f}(\boldsymbol{w}, z)$. If other sensors, such as LiDAR, are used to obtain accurate ground phase and tree height as the initial values of PCT algorithm, the effects of propagating errors from tree height and ground phase on PCT algorithm can be reduced and the performance of $\hat{f}(\boldsymbol{w}, z)$ reconstruction should be further improved to further improve accuracy of AGB estimation.

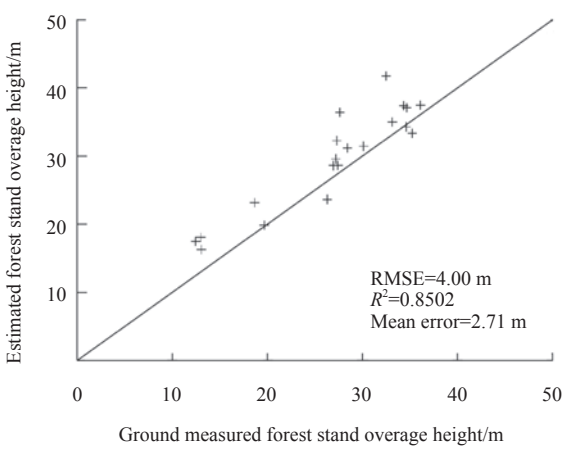

Fig. 6 the scatter diagram of ground measured average forest stand height with estimated average forest stand height by the phase-amplitude hybrid inversion method based on interferometric coherence optimization without non-volumetric decorrelation compensation

4.2.3 Compared with the AGB estimation method only based on the forest stand average height

Forest stand average height inversed from PolInSAR data may be directly used to do stepwise regression analysis with ground measured stand average AGB to construct AGB estimation model. Based on the forest stand average heights $\hat{h}_m$ estimated by the method described in section 3.1, the AGB estimation model is constructed as Eq. (8) and the corresponding results are shown by model 4 (M4) in Table 2. The scatter plot is shown in Fig. 7 with R^2 of 0.9031 and RMSE of 0.21 t/hm^2. This shows M4 generally gives poor results than that of M1.

$$\ln B = -0.5270 + 1.8457 \ln(\hat{h}_m) \quad (8)$$

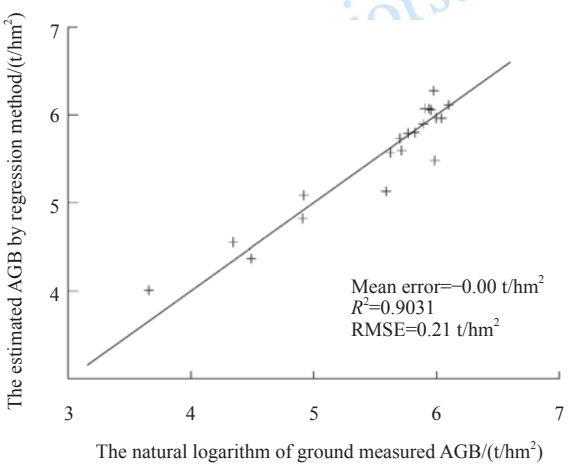

Fig. 7 Scatter diagram of ground measured AGB (natural logarithm) with the estimated AGB (natural logarithm) by stepwise regression method using only the estimated forest stand average heights

The predictive values from M1 and M4 are taken inverse functions of natural logarithm and are plotted against ground measured forest stand AGB as shown in Fig. 8 (a) and (b), respectively. It can be seen that compared with R^2 of the AGB estimation mode only based on forest stand average heights, R^2 of the AGB estimation model based on the relative reflectance function increases from 0.8219 to 0.8630 and RMSE decreases from 57.59 t/hm^2 to 47.86 t/hm^2. Then 10-fold cross validation is used to compare AGB estimation accuracy of M1 and M4. The results of cross validation show that the average prediction error of the biomass decreases from 3.97 t/hm^2 to 0.17 t/hm^2. Therefore, we can conclude that the three parameters closely related with forest structure information have greater explanatory ability for AGB than a single forest stand average height

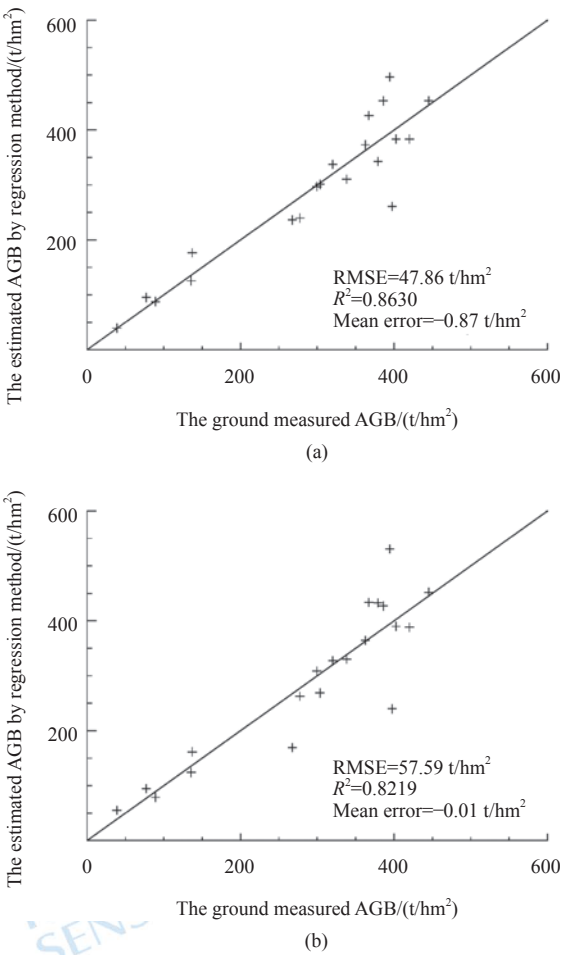

Fig. 8 Scatter diagram of ground measured AGB with the estimated AGB by stepwise regression method
(a) Using the characteristic parameters; (b) Using only the estimated forest stand average heights

and can be used to improve performance of the AGB estimation.

Estimated AGB of the 20 validate stands by M1 are mapped as shown in Fig. 9(a). Fig. 9(b) shows the corresponding ground measured forest stand average AGB. It can be seen that estimation results using M1 can well reflect the actual spatial variation of forest AGB.

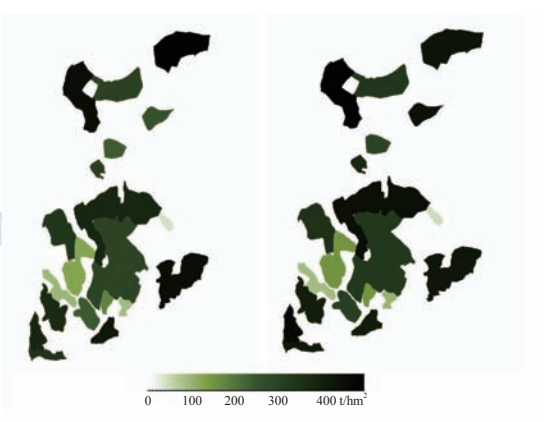

Fig. 9 Forest stands average AGB map
(a) Estimated by M1; (b) Ground measured

5 CONCLUSIONS

In this paper, the advantage and potential of forest stand average AGB estimation model and method using PCT technology is investigated with the repeat pass ESAR L-band PolInSAR data collected by DLR at the Traunstein test site. Ground measured forest stands AGB of the 20 validate stands by the detailed forest inventory are used to quantitatively analyze and evaluate the main factors affecting the AGB estimation with the developed model and methods. The main conclusions are as follows:

(1) Based on the analysis of relative reflectivity function curve of different levels of typical stand AGB, the nine characteristic parameters, which are possibly correlated with forest stand AGB, are defined and used to do correlation analysis with the 20 ground measured forest stands AGB. The results show that except the 9th parameter, the other 8 parameters have good correlation with forest stand AGB.

(2) Based on the stepwise regression analysis with the forest stand average characteristics arguments as independent variables and ground measured forest stand average AGB as the dependent variable, the model and method for AGB estimation are proposed. The effects of choice of polarization channel and estimation error of the tree height on performance of the AGB estimation model are analyzed. The results show that the AGB estimation model based on relative reflectivity function in polarization channel dominated by volume scattering is superior to that in polarization channel dominated by surface scattering. Accurate tree height estimation is very important for estimation of forest stand AGB based on PCT. Estimation error of tree height will decrease the accuracy of AGB estimation.

(3) The AGB estimation method based on the characteristic parameters from the relative reflectivity function is compared with that only based on the forest stand average height and the results show that R^2 is increased from 0.8219 to 0.8630, while RMSE is decreased from 57.59 t/hm^2 to 47.86 t/hm^2. The results of cross validation show that the average error is reduced from 3.97 t/hm^2 to 0.17 t/hm^2, which indicates that the characteristic parameters extracted from the relative reflectance functions based on PCT technology are sensitive to the biomass and making full use of information from relative reflectivity function can improve the accuracy of AGB estimation.

Acknowledgements: The experimental data used in the study are provided under the contract of the Dragon 2 program between the MOST (China Ministry of Science Technology) and ESA (European Space Agency). We are grateful to them for their help.

REFERENCES

Bai L, Cao F and Hong W. 2010. Fast approach to estimate the longest axis in coherence region and its applications. *Journal of Electronics and Information Technology*, **32**(3): 548–553 DOI: 10.3724/SP.J.1146.2009.00211

Chen E X. 1999. Development of forest biomass estimation using SAR data. *World Forestry Research*, **12**(6): 18–23

Chen X, Zhang H and Wang C. 2009. The inversion of vegetation structural parameters using dual-baseline polarimetric SAR interferometry. *Remote Sensing for Land and Resources*, **20**(4): 49–52

Cloude S R and Papathanassiou K P. 2008. Forest vertical structure estimation using coherence tomography. IEEE International Geoscience and Remote Sensing Symposium. Boston, MA, USA: V-275-V-278

Cloude S R. 2006. Polarization coherence tomography. *Radio Science*, **41**(4): RS4017.1–RS4017.27

Cloude S R and Papathanassiou K P. 2003. Three-stage inversion process for polarimetric SAR interferometry. *IEE Proceedings-Radar*, *Sonarand Navigation*, **150**(3): 125–134 DOI: 10.1049/ip-rsn:20030449

Dobson M C, Ulaby F T, Pierce L E, Sharik T L, Bergen K M, Kellndorfer J, Kendra J R, Li E, Lin Y C, Nashashibi A, Sarabandi K and Siqueira P. 1995. Estimation of forest biophysical characteristics in Northern Michigan with SIR-C/X-SAR. *IEEE Transactions on Geoscience and Remote Sensing*, **33**(4): 877–895 DOI: 10.1109/36.406674

Feng Z k and Liu Y X. 2005. Precision analysis of forest biomass measuring. *Journal of Beijing Foresrry University*, **27**(S2): 108–111

Gao H X. 2005. Application of Multivariate Statistical Analysis. Beijing: Beijing University Press

Lu D S. 2006. The potential and challenge of remote sensing-based biomass estimation. *International Journal of Remote Sensing*, **27**(7): 1297–1328 DOI: 10.1080/01431160500486732

Luo H M, Chen E X, Cheng J and Li X W. 2010a. Forest height estimation methods using polarimetric SAR interferometry. *Journal of Remote Sensing*, **14**(4): 814–830

Luo H M, Li X W, Chen E X, Cheng J and Cao C X. 2010b. Analysis of forest backscattering characteristics based on polarization coherence tomography. *Science China Technological Sciences*, **53**(S1): 166–175 DOI: 10.1007/s11431-010-3242-y

Mette T. 2007. Forest Biomass Estimation from Polarimetric SAR Interferometry. Munich: Munich University of Technology

Praks J, Kugler F, Hyyppa J, Papathanassiou K and Hallikainen M. 2008. SAR coherence tomography for boreal forest with aid of laser measurements. IEEE International Geoscience and Remote Sensing Symposium, Boston: II-469-II-472 DOI: 10.1109/IGARSS.2008.4779030

Ranson K J, Sun G, Weishampei J F and Knox R G. 1997. Forest biomass from combined ecosystem and radar backscatter modeling. *Remote Sensing Environment*, **59**(1): 118–133 DOI: 10.1016/S0034-4257(96)00114-9

Steininger M K. 2000. Satellite estimation of tropical secondary forest aboveground biomass: data from Brazil and Bolivia. *International Journal of Remote Sensing*, **21**(6-7): 1139–1157

Tabb M, Orrey J, Flynn T and Carande R. 2002. Phase diversity: a decomposition for vegetation parameter estimation using polarimetric SAR interferometry. Proceedings of 4th European Synthetic Aperture Radar Conference (EUSAR 2002). Cologne

Treuhaft R N, Asner G P, Law B E and van Tuyl S. 2002. Forest leaf area density profiles from the quantitative fusion of radar and hyperspectral data. *Journal of Geophysical Research*, **107**(D21): 4568–4580

Treuhaft R N, Asner G P and Law B E. 2003. Structure-based forest biomass from fusion of radar and hyperspectral observations. *Geophysical Research Letters*, **30**(9): 1472–1475

Treuhaft R N, Chapman B D, dos Santos J R, Goncalves F G, Dutra L V, Graca P M L A and Drake J B. 2009a. The ambiguity in forest profiles and extinction estimated from multibaseline interferometric SAR. *Boletim de Ciências Geodésicas*, **15**(3): 299–312

Treuhaft R N, Chapman B D, dos Santos J R, Goncalves F G, Dutra L V, Graca P M L A and Drake J B. 2009b. Vegetation profiles in tropical forests from multibaseline interferometric synthetic aperture radar, field, and lidar measurements. *Journal of Geophysical Research*, **114**(D23): D23110.1- D23110.16

Wang C L, Guo Z X, Niu Z and Lin W P. 2006. Study on forest biophysics parameter impact on RADARSAT SAR signature. *Ecology and Environment*, **l5**(1): 115–119

Xu X J, Du H Q, Zhou G M and Fan W Y. 2008. Review on correlation analysis of independent variables in estimation models of vegetation biomass based on remote sensing. *Remote Sensing Technology and Application*, **23**(2): 239–247

Yang C J, Liu J Y, Huang H, Xu H X and Dang C L. 2005. Correlation analysis of the biomass of the tropical forest vegetation, meteorological data and topographical data. *Geographical Research*, **24**(3): 473–479

森林地上生物量的极化相干层析估计方法

罗环敏[1]，陈尔学[2]，李增元[2]，曹春香[3]

1. 电子科技大学 地表空间信息技术研究所，四川 成都 610054；
2. 中国林业科学研究院 资源信息研究所，北京 100091；
3. 遥感科学国家重点实验室 中国科学院遥感应用研究所，北京 100101

摘　要：基于微波的后向散射系数估计森林地上生物量(AGB)易受后向散射系数饱和的影响，而利用森林高度，根据生长方程估计AGB，却没有考虑和AGB密切相关的林分密度、树种组成、林层垂直分布等空间结构特征的作用，针对这些问题，提出一种基于极化相干层析(Polarization Coherence Tomography，PCT)技术的AGB估计方法。基于德国宇航局(DLR)机载SAR系统(ESAR)获取的特劳斯坦(Traunstein)试验区L-波段极化干涉SAR(PolInSAR)数据，通过对具有不同AGB水平的典型林分的相对反射率函数曲线的分析，定义了9个与AGB具有相关性的特征参数。然后基于20个林分的实测AGB数据，以林分尺度上这9个特征参数的平均值为自变量，以实测林分平均AGB为因变量，采用逐步回归分析法构建了AGB估测模型，并对该模型进行评价，对影响模型估计精度的因素进行分析，结果表明，由PCT提取的相对反射率函数特征参数对AGB很敏感，充分利用相对反射率函数信息可提高AGB估计精度。

关键词：极化干涉SAR，极化相干层析，逐步回归分析法，森林地上生物量

中图分类号：TN957.51　　**文献标志码：**A

引用格式：罗环敏，陈尔学，李增元，曹春香. 2011. 森林地上生物量的极化相干层析估计方法. 遥感学报，**15**(6): 1138–1155
Luo H M, Chen E X, Li Z Y and Cao C X. 2011. Forest above ground biomass estimation methodology based on polarization coherence tomography. *Journal of Remote Sensing*, **15**(6): 1138–1155

1　引　言

森林地上生物量AGB的大区域准确估计对全球碳循环及气候变化研究具有重要意义。很多学者开展了遥感森林AGB估测研究(陈尔学，1999；杨存建 等，2005；徐小军 等，2008；Lu，2006)，常用的方法是利用微波的极化后向散射系数、光学的波谱反射率等遥感参数和生物量之间建立经验或半经验关系模型，但当AGB水平过高时，就会出现信号饱和问题(王臣立 等，2006；Ranson 等，1997；Dobson 等，1995；Steininger，2000)。近几年来迅速发展起来的PolInSAR、激光雷达(LiDAR)技术可估测出树高，基于反演得到的树高，根据生长方程就可间接推算出AGB，这种方法在一定程度上解决了AGB遥感估测的信号饱和问题(Mette，2007)[112,121]。但森林AGB除了与树高有密切关系外，还受林分密度、树种组成和林层垂直分布等空间结构特征的影响。因此可以推测，如果在AGB估测中综合考虑林分的垂直结构信息，应该可以进一步提高森林AGB估计精度。

然而，不同的研究领域(如森林经理学和森林生态学等)和不同学者对森林垂直结构信息的描述及地面观测方法都可能不同，但用于描述森林垂直结构信息的参数(M)有一个共同的特点，即M是随高度z变化的，可抽象为一个函数$M(z)$。比如，用于描述森林叶面积随高度变化的叶面积密度(LAD)就是具有该特点的一种森林垂直结构参数。如果$M(z)$可以精确测量，

收稿日期：2010-11-08；**修订日期：**2011-01-30

基金项目：国家重点基础研究重点计划(973 计划) (编号: 2007CB714404)；国家自然科学基金 (编号: 60890074)

第一作者简介：罗环敏(1972—)，男，博士研究生，2005年毕业于电子科技大学测试计量技术与仪器专业, 获硕士学位，现从事极化干涉SAR理论和应用研究，已发表论文6篇。E-mail: Lhm123345@qq.com。

通信作者简介：陈尔学(1968—)，男，研究员，2004年获中国林业科学研究院博士学位，现主要从事雷达遥感理论和应用研究，最近5年发表雷达遥感应用领域论文10余篇。E-mail: chenerx@caf.ac.cn。

森林蓄积量V和AGB等代表森林综合结构的参数就可以精确估测。采用遥感的手段可以反演出与森林垂直结构密切相关的一个物理量随z的垂直分布$E(z)$，但$E(z)$不等同于$M(z)$，只有建立起遥感反演物理量$E(z)$与$M(z)$或与V、AGB等之间的关系，才能估测出用户所关心的专题信息，如$M(z)$、V和AGB等。

基于SAR成像数据反演的雷达相对反射率函数(Relative reflectivity function)$f(z)$是上面所述$E(z)$的一种具体形式，目前国内外已报道的反演$f(z)$的方法主要有两种，一是Treuhaft等人(2009a，2009b)利用C-波段多基线InSAR反演$f(z)$。该方法基于包含垂直结构函数的相干散射模型，利用多个高度上的基线相干矢量，找出使模型预测相干值和观察相干值相差最小的结构参数，从而得到假设为高斯分布的$f(z)$。二是Cloude(2006)[1-25]利用PolInSAR数据采用极化相干层析反演$f(z)$。PCT利用极化干涉相干对森林结构变化的敏感性，在每个像元上把$f(z)$用傅里叶-勒让德级数展开，然后用干涉相干估计其系数，重构$f(z)$，这种方法并没有像第一种方法那样假设$f(z)$为高斯分布。

在将多基线C-波段InSAR提取的$f(z)$应用于$M(z)$和AGB反演方面，Treuhaft等人(2002，2003)做了大量的工作。Treuhaft等人(2002)将InSAR反演的$f(z)$与高光谱遥感提取的LAI相结合，得到LAI的垂直分布(LAD)信息，LAD类似于前面所述的$M(z)$，并将其与地面实测数据进行了对比，发现有较好的一致性。Treuhaft等人(2003)进一步将LAD用于AGB的估计，取得了较好的效果。而在PCT的应用方面，虽然Cloude(2006)[25]在发表PCT文章时就已经指出了PolInSAR反演的$f(z)$在AGB估测中具有潜在的应用价值，随后也有学者从不同的角度进行了探索(陈曦 等，2009；Cloude和Papathanassiou，2008；Luo 等，2010b；Praks 等，2008)，但目前尚缺乏将其应用于森林AGB估测的研究报道。有鉴于此，本文基于利用德国宇航局(DLR)机载SAR系统(ESAR)获取的特劳斯坦(Traunstein)实验场L-波段单基线PolInSAR数据，深入研究了基于PCT反演的雷达相对反射率函数估测森林AGB的方法。

2 试验区及数据获取情况

试验区位于德国南部城市特劳斯坦附近，地形平坦，海拔在600—650 m之间，主要地表覆盖类型为城镇、道路、农田、森林和牧场。试验区森林优势树种类型以云杉(Picea abies)、山毛榉(Fagus sylvatica)和冷杉(Abies alba)为主。2003-10-11，DLR利用ESAR系统获取了覆盖该试验区的L-波段PolInSAR数据。飞机平均航高为3 km，近距入射角为25°，远距入射角为60°，距离向、方位向分辨率分别为1.5 m、3.0 m。采用重复飞行方式获取干涉SAR(InSAR)数据，标称空间基线为5 m，时间基线为20 min。DLR已将数据配准，并提供了平地相位和有效波数影像，所获取的InSAR像对的主影像Pauli极化基RGB彩色组合显示见图1，红色表示HH极化和VV极化响应的差，反应偶次散射的强弱；如城镇部分；蓝色表示HH极化与VV极化响应的和，反应奇次散射的强弱；绿色表示HV极化的响应，反应体散射的强弱。可以看到，在森林区，体散射很强。雷达的方位向与图1中红线平行(从上向下)。在飞行试验期间对20个林分进行了详细的样地抽样调查，根据样地抽样调查数据分别林分计算得到平均优势高h_m，其含义是每公顷林分中最高的100株树的算术平均高，这里简称林分平均高。并利用生长方程计算出每个林分的AGB作为地面测量林分平均AGB(Mette，2007)[35,36]，其变化范围为38.7—445.2 t/hm^2。

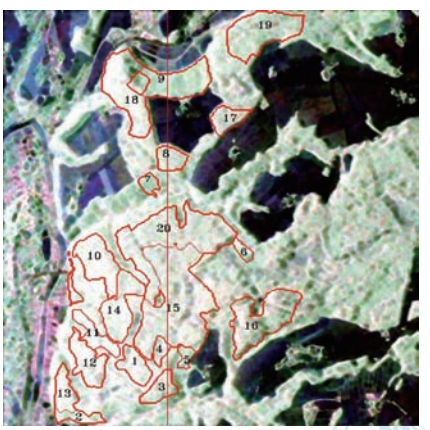

图1 德国特劳斯坦实验区极化SAR数据的Pauli极化基RGB彩色组合图

3 原理与方法

3.1 基于PCT的森林相对反射率函数反演方法

Cloude(2006)[7-25]对PCT算法进行了详细的论述，这里仅介绍其主要方法。设位于InSAR系统空间基线1、2两端的SAR传感器获取的地面森林植被的复信号为$\boldsymbol{S}_1$和$\boldsymbol{S}_2$，两者之间的复相干可用式(1)表示。

$$\tilde{\gamma}_{\boldsymbol{w}}=\frac{\left\langle \boldsymbol{s}_1\boldsymbol{s}_2^{*}\right\rangle}{\sqrt{\left\langle \boldsymbol{s}_1\boldsymbol{s}_1^{*}\right\rangle\left\langle \boldsymbol{s}_2\boldsymbol{s}_2^{*}\right\rangle}}=\mathrm{e}^{\mathrm{i}\phi_0}\frac{\int_0^{h_v}f(\boldsymbol{w},z)\mathrm{e}^{\mathrm{i}k_z z}\mathrm{d}z}{\int_0^{h_v}f(\boldsymbol{w},z)\mathrm{d}z}$$

$$0\leqslant|\tilde{\gamma}|\leqslant 1 \tag{1}$$

式中，ϕ_0是地形相位；垂直波数$k_z=\dfrac{4\pi\Delta\theta}{\lambda\sin\theta}$，$\theta$为入射角；$\Delta\theta$为两干涉影像的入射角差异，$\lambda$为入射波波长；$h_v$为像元内的平均树高；$f(w, z)$代表某一种极化状态($\boldsymbol{w}$)下随植被垂直高度$z$而变化的雷达相对反射率。$z$的最小值为0，对应林下地形的高程；最大值为$h_v$。对极化干涉SAR影像进行PCT处理，可由式(2)得到$f(\boldsymbol{w}, z)$的估计：

$$\hat{f}_{L2}(\boldsymbol{w},z)=\frac{1}{\hat{h}_v}\Big(1-\hat{a}_{10}(\boldsymbol{w})+\hat{a}_{20}(\boldsymbol{w})+\frac{2z}{\hat{h}_v}(\hat{a}_{10}(\boldsymbol{w})-3\hat{a}_{20}(\boldsymbol{w}))+\hat{a}_{20}(\boldsymbol{w})\frac{6z^2}{\hat{h}_v^2}\Big)$$

$$(0\leqslant z\leqslant\hat{h}_v) \tag{2}$$

式中，$L2$表示对$f(\boldsymbol{w}, z)$的勒让德多项展开式在二阶进行截断得到的估计，为叙述方便下文将省略该下标符号；$\hat{h}_v$是h_v的估计值；勒让德多项式系数$\hat{a}_{10}(\boldsymbol{w})$和$\hat{a}_{20}(\boldsymbol{w})$可由式(3)估计：

$$\hat{a}_{10}(\boldsymbol{w})=\frac{\mathrm{Im}(\tilde{\gamma}_k)}{f_1}$$

$$\hat{a}_{20}(\boldsymbol{w})=\frac{\mathrm{Re}(\tilde{\gamma}_k)}{f_2}-\frac{f_0}{f_2}$$

$$\tilde{\gamma}_k=\tilde{\gamma}(\boldsymbol{w})\mathrm{e}^{-\mathrm{i}(\hat{k}_v+\hat{\phi}_0)}$$

式中，

$$k_v=\frac{k_z\hat{h}_v}{2}\quad f_0=\frac{\sin k_v}{k_v}\quad f_1=\mathrm{i}\Big(\frac{\sin k_v}{k_v^2}-\frac{\cos k_v}{k_v}\Big)$$

$$f_2=\frac{3\cos k_v}{k_v^2}-\Big(\frac{6-3k_v^2}{2k_v^3}+\frac{1}{2k_v}\Big)\sin k_v \tag{3}$$

由此可见，只要估计出树高$\hat{h}_v$和地形相位$\hat{\phi}_0$，对于极化状态$\boldsymbol{w}$，计算出相应的相干$\tilde{\gamma}(\boldsymbol{w})$，便可求出$k_v$和$\tilde{\gamma}_k$，进而求出勒让德多项式系数$\hat{a}_{10}(\boldsymbol{w})$和$\hat{a}_{20}(\boldsymbol{w})$，由式(2)重构该极化状态下各像元的相对反射率函数$\hat{f}(\boldsymbol{w}, z)$。

由此可见，树高和相应的林下地形相位是结构函数重构的两个关键输入参数，其估计误差的大小直接影响相对反射率函数重构的精度。利用极化干涉数据提取树高，有很多种方法(Cloude和Papathanassiou，2003；白璐 等，2010)，对于特劳斯坦实验场的L-波段PolInSAR数据，各极化通道间相干相位相差不大，且存在非体散射去相干，在树高估计中，如果仅利用相干相位信息，会出现低估现象；而若只利用相干幅度信息，则会发生高估现象。为提高树高估测精度，本文采用了基于极化相干优化和非体散射去相干补偿的幅度-相位综合反演方法(罗环敏 等，2010)[819,820]。干涉像对数据经过配准、平地相位去除、多视处理和滤波处理后，用相位分离最大相干优化方法计算体散射去相干$\tilde{\gamma}(\boldsymbol{w}_v)$和表面散射去相干$\tilde{\gamma}(\boldsymbol{w}_s)$(Tabb 等，2002)，进而求出地形相位$\hat{\phi}_0$ (Cloude，2006)[6]，再考虑校正非体散射去相干因子R_d的影响，就可以基于相干幅度和相位信息估计出$\hat{h}_v$，罗环敏等人(2010)[818-820]详细地描述了这些步骤。采用这种反演方法估计的树高在图1中红色多边形所示的林分内求算术平均，得到每个林分的林分平均高估计值，和实地测量的林分平均高之间的散点图见图2，估测值与实测值之间的相关系数平方R^2为0.8630，平均误差为0.90 m，均方根误差(RMSE)为3.11 m。

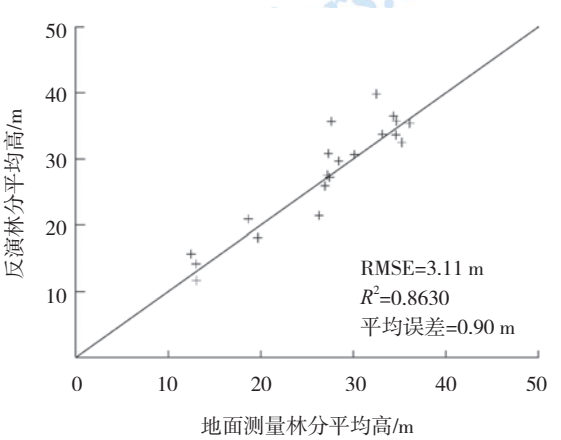

图2 基于极化相干优化和非体去相干补偿的相干相位-幅度法求算的林分平均高与地面实测林分平均高的散点图

对森林覆盖区像元进行PCT反演，得到像元的体散射占主导作用极化通道的$\hat{f}(\boldsymbol{w}, z)$。对获得的$\hat{f}(\boldsymbol{w}, z)$，沿图1中的红线做一个剖面，对剖面上的$\hat{f}(\boldsymbol{w}, z)$值(在0—0.25之间)做颜色映射，得到层析剖面图(图3)，其横轴代表图1中沿红直线的像元号，纵轴表示垂直高度，用不同颜色表示相对反射率强弱，可以看出森林上层由体散射贡献的相对反射率随着穿透深度的增加逐渐衰减，在森林接近地表层也有较强的由体散射引起的相对反射率，说明林下可能有较茂密的灌木层存在。

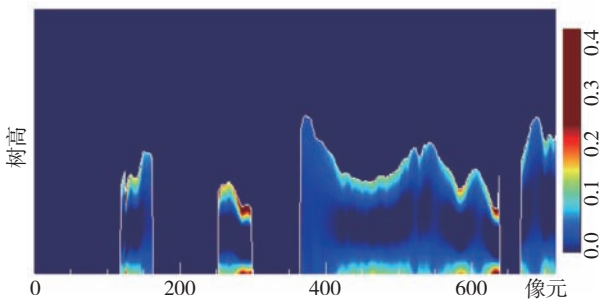

图3 PCT处理得到的相对反射率在方位向(沿图1中红线)的垂直剖面图

3.2 林分平均相对反射率函数的计算及其特征参数的定义

由式(2)计算得到的是像元的$\hat{f}(\boldsymbol{w}, z)$，而地面实测森林AGB数据是按林分提供的，代表的是一个林分的平均AGB，因此需要按林分计算平均$\hat{f}(\boldsymbol{w}, z)$。图1中用红色多边形绘出了20个实测林分的边界，对落入某个林分内的所有像元的$\hat{f}(\boldsymbol{w}, z)$求算术平均就得到该林分的平均$\hat{f}(\boldsymbol{w}, z)$，每个林分对应一个平均$\hat{f}(\boldsymbol{w}, z)$。后文的分析将全部基于林分的平均$\hat{f}(\boldsymbol{w}, z)$进行。

图4分别代表低(14号林分：AGB为135.7 t/hm^2)、中(9号林分：AGB为303.3 t/hm^2)和高(20号林分：AGB为402.6 t/hm^2)3个级别AGB的林分的$\hat{f}(\boldsymbol{w}, z)$。图中，$h_2$和$h_4$代表$\hat{f}(\boldsymbol{w}, z)$上半部分中相对反射率最接近0.002的高度，在$h_2$和$h_4$之间的数据构成第1个包络，$h_3$是第1个包络的峰值对应的高度。在$\hat{f}(\boldsymbol{w}, z)$下半部分中，最大相对反射率和$h_2$之间的第1个拐点所对应的高度用$h_1$表示，在$h_1$和0之间的数据构成第2个包络。可以看出，第1个包络的形状和位置与AGB密切相关，对于AGB高的林分，如20号，峰值小，包络的跨度(即h_4–h_2)大，h_3的值大，第2个包络的最大值和较低级别AGB的林分(如14号)相比较小。对曲线的上半部分做高斯函数拟合，拟合高斯函数的曲线如图中的红虚线所示，拟合曲线能很好地和$\hat{f}(\boldsymbol{w}, z)$上半部分曲线吻合，说明在林分尺度上，平均相对反射率函数的上半部分呈高斯分布。

为了定量分析$\hat{f}(\boldsymbol{w}, z)$与森林AGB之间的关系，定义了9个用于描述$\hat{f}(\boldsymbol{w}, z)$曲线特征的参数，具体如下：

参数1：$P_1=(h_4-h_2)/\hat{f}(\boldsymbol{w}, h_3)$，表示第1个包络的跨距除以其峰值；

参数2：$P_2=\sum_{z=h_2}^{z=h_4} z\cdot\hat{f}(\boldsymbol{w}, z)$，表示第1个包络中，将每一个幅值和对应高度相乘，然后再求和；

参数3、4、5：对第1个包络进行高斯拟合，其幅度的倒数、均值和方差分别记作P_3、P_4、P_5；

参数6：$P_6=1/\sum_{z=h_2}^{z=h_4}\hat{f}(\boldsymbol{w}, z)$，表示第1个包络的幅值之和的倒数；

参数7：$P_7=1/\sum_{z=0}^{z=h_1}\hat{f}(\boldsymbol{w}, z)$，表示第2个包络的幅值

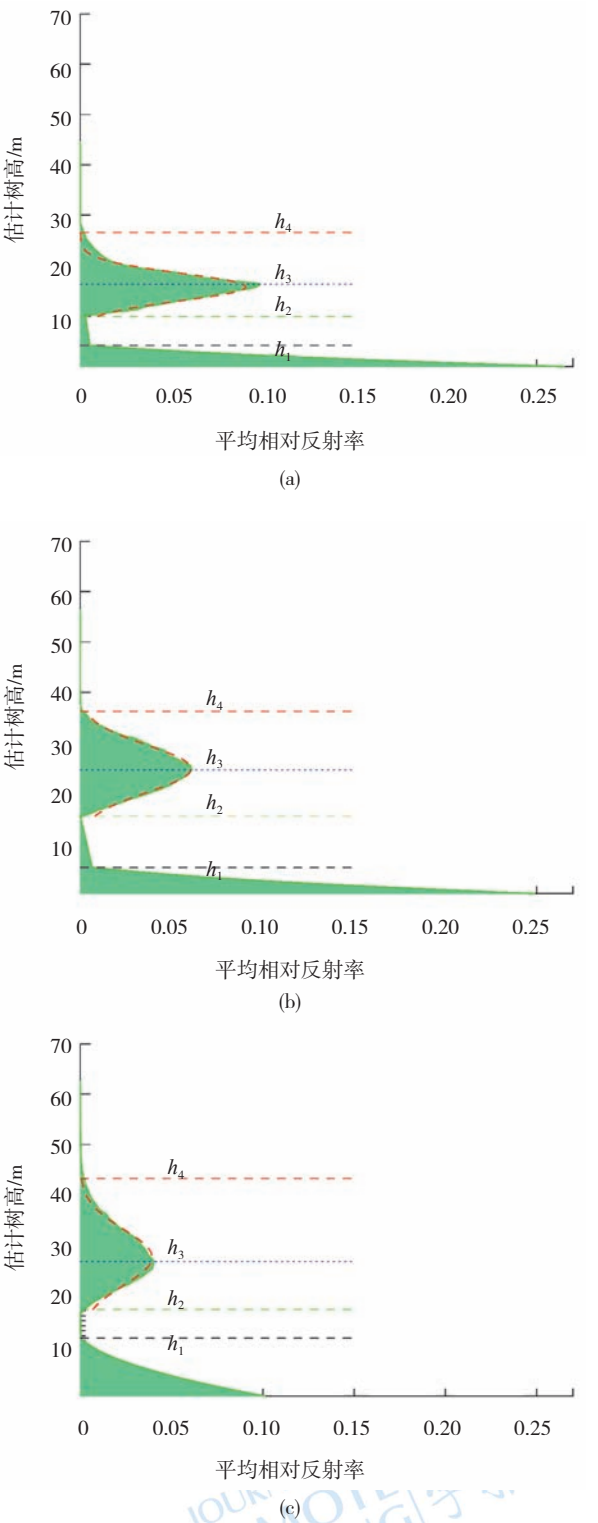

图4 在体散射占主导作用的极化通道3块典型林分的平均相对反射率函数
(a) 14号样地；(b) 9号样地；(c) 20号样地

之和的倒数；

参数8：$P_8=P_6/P_7$；

参数9：$P_9=\sum_{z=h_2}^{z=h_3}\hat{f}(\boldsymbol{w},z)/\sum_{z=h_3}^{z=h_4}\hat{f}(\boldsymbol{w},z)$，表示对于第1个包络，以$h_3$为界限，下半部分幅值之和除以上半部分幅值之和。

3.3 森林地上生物量估测模型

有研究表明，用式(4)的幂函数形式描述AGB和SAR遥感观测值之间的关系具有较高的相关性(冯仲科和刘永霞，2005)，因此本文也采用式(4)作为估测森林AGB的模型。

$$B=b_0'\prod_{i=1}^{n}P_i^{b_i} \tag{4}$$

式中，B为AGB，P_i为自$\hat{f}(\boldsymbol{w},z)$提取的特征参数，$b_0'$和$b_i$为模型参数，$n$为模型中采用的$\hat{f}(\boldsymbol{w},z)$特征参数的个数。本文定义了9个特征参数，所以$n$的最大值可为9。对式(4)两边取自然对数，

$$\ln(B)=\ln(b_0')+b_1\ln(P_1)+b_2\ln(P_2)+\cdots+b_n\ln(P_n)$$

设

$$Y=\ln(B),\ b_0=\ln(b_0'),$$
$$X_1=\ln(P_1),\ X_2=\ln(P_2),\ \cdots,\ X_n=\ln(P_n) \tag{5}$$

则得到如下多元一次线性方程：

$$Y=b_0+b_1X_1+b_2X_2+\cdots+b_nX_n \tag{6}$$

3.4 生物量估测模型的建立与评价方法

采用多元线性逐步回归分析方法建立式(6)所示的AGB估测模型，目的是筛选出对森林AGB估测有显著作用的特征参数P，找到最佳自变量组合建立回归方程来预测因变量(高惠璇，2005)。该方法将特征参数自变量由少到多依次引入回归方程，在每次引入一个变量后，都要分析已引入方程中的变量，剔除作用不显著的，直到没有一个自变量能引入方程和没有一个自变量能从方程中剔除，最后保留下来的变量就是对因变量估测贡献最大、影响最显著的变量，而被剔除的变量对因变量的影响较小，即解释因变量的能力较弱。

在逐步回归分析中，必须避免方程出现严重共线性问题。自变量间的严重共线性会使模型失去意义，衡量共线性程度常用容差或方差膨胀因子，一个自变量的容差是指其解释的方差中不能由方程中其他自变量解释的部分所占的比例，而方差膨胀因子是容差的倒数，容差越接近于0或方差膨胀因子越大，共线性程度就越强。

回归模型的一致性和显著性用R^2和统计量F及P值来评定，F值为回归均方与残差均方的比值，查F界值表，可得到相应的P值，从而在给定的水平，对方程进行回归显著性判断。

3.5 生物量估测模型的精度检验方法

为了评价通过逐步回归法建立的AGB估测模型的精度，采用m重交叉验证法(m-fold cross-validation)，即将N个样本分成m等份，用$G_1, G_2, G_3, \cdots, G_m$表示，将其中一份作为精度检验样本$G_v$，剩余的作为模型建立用样本$G_t$。对每一份$G_i(i=1, 2, \cdots, m)$样本都执行一次该过程，共需要重复$m$次，最终得到$N$个样本的估测值，利用这$N$个样本的估测值和实测值计算$R^2$和RMSE作为模型性能的评价指标。本文样地数为20，则N=20，m设为10。

4 结果与分析

4.1 生物量估测模型建立与分析

在体散射占主导作用的极化通道$\boldsymbol{w}_v$，用3.1节中所描述的方法，获得各实测林分的平均$\hat{f}(\boldsymbol{w},z)$，并提取出9个特征参数与AGB做相关性分析，计算得到的相关系数R见表1。可以看出，这些参数在一定程度上都和生物量相关，其中，高斯拟合的3个参数(P_3, P_4, P_5)相关性最强。

进一步将这9个参数和AGB做逐步回归分析，在逐步引入-剔除法进行变量的选择中，用统计量F的显著性概率值即P值来判定，如果候选自变量中最大F值的P值小于或等于0.05，则相应的自变量就进入模

表1 三种不同处理方法提取的特征参数和生物量之间的相关系数

方法＼参数	P_1	P_2	P_3	P_4	P_5	P_6	P_7	P_8	P_9
方法1	0.8698	0.7041	0.9136	0.9355	0.8886	0.7627	0.7583	0.6487	0.2414
方法2	0.8668	0.7486	0.9196	0.9402	0.8928	0.7828	0.7952	0.6659	0.2743
方法3	0.8426	0.7229	0.8800	0.9281	0.8086	0.4783	0.6513	0.3255	0.5747

注：方法1：在体散射占主导作用的极化通道，并进行了非体散射去相干补偿；方法2：在表面散射占主导作用的极化通道，并进行了非体散射去相干补偿；方法3：在体散射占主导作用的极化通道，没有进行非体散射去相干补偿

型，对于已进入方程中的自变量，最小F值的P值如果大于或等于0.051，相应的自变量就被剔除。最后选择出3个自变量：P_4、P_8和P_9，相应的回归分析结果如表2中的模型1(M1)。

M1中各自变量的容差均较大(大于0.5)，方差膨胀因子很小(小于2)，说明这3个自变量间不存在共线性问题。回归方程显著性检验F=95.9768，显著性水平值P=0.0000，表明回归模型是显著的、有意义的。根据偏回归系数构建AGB回归方程如式(7)。

$$\ln B=-2.9966+1.7806\ln(P_4)+0.5765\ln(P_8)-0.2927\ln(P_9) \quad (7)$$

利用式(7)估测的与实测的林分平均AGB(自然对数值)

表2 生物量估测的逐步回归分析结果比较

模型	模型参数	R^2	调整的相关系数平方(R_1^2)	参数估测值	F值	P值	共线性统计量	
							容差	方差膨胀因子(VIF)
M1		0.9474	0.9375	b_0=−2.9966	95.9768	0.0000		
	P_4			b_4=1.7806			0.5453	1.8340
	P_8			b_8=0.5765			0.6876	1.4544
	P_9			b_9=−0.2927			0.7067	1.4149
M2		0.9479	0.9381	b_0=−0.7766	97.0290	0.0000		
	P_4			b_4=1.8960			0.3153	3.1715
	P_8			b_8=2.3706			0.2053	4.8714
	P_7			b_7=−2.1366			0.1121	8.9168
MM2		0.9287	0.9203	b_0=−1.3218	110.7269	0.0000		
	P_4			b_4=1.5424			0.7337	1.3629
	P_8			b_8=1.1565			0.7337	1.3629
M3		0.8932	0.8806	b_0=−4.8165	71.0603	0.0000		
	P_4			b_4=1.9590			0.7081	1.4122
	P_7			b_7=0.8827			0.7081	1.4122
M4	$\hat{h}_v$	0.9031	0.8977	b_0=−0.5270	167.7714	0.0000	1	1
				b_1=1.8457				

注：模型参数精确到小数点后4位

M1：在体散射占主导作用的极化通道，用逐步引入–剔除回归方法对提取的9个参数进行回归分析，构建的模型

M2：在表面散射占主导作用的极化通道，用逐步引入–剔除回归方法对提取的9个参数进行回归分析，构建的模型

MM2：针对模型2，去除引起共线性的变量P7，进行回归分析，构建的模型

M3：在体散射占主导作用的极化通道，估计森林高度时不考虑非体去相干因子，用逐步引入–剔除回归方法对提取的9个参数进行回归分析，构建的模型

M4：利用相干幅度–相位信息反演林分平均高，并和生物量进行回归分析，构建的模型

之间的散射点图见图5，RMSE=0.15 t/hm^2，大部分点落在1:1直线上，小部分均匀地分布在直线的两侧；模型R^2高达0.9474，消除自变量的个数及样本量的大小对R^2的影响后，得到调整的相关系数平方R_1^2，仍然高达0.9375，这些都说明因变量和这3个自变量存在很好的相关性。

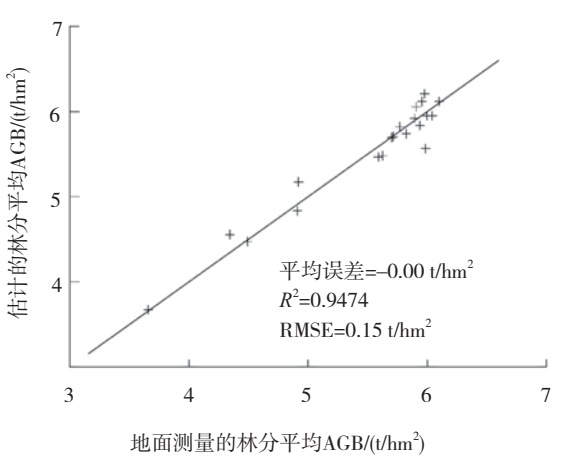

图5 逐步回归模型估计与地面实测林分平均AGB(自然对数值)的散点图

从方程参数估测值的符号还可以看到，P_4和P_8对AGB估测的影响是正向的，其值越大，AGB估测值就越大，而P_9则刚好相反，这和图4所反映的情况一致。

4.2 影响AGB估测模型的因素分析

基于PCT估测的$\hat{f}(\boldsymbol{w}, z)$和极化密切相关，不同的极化状态下，$\hat{f}(\boldsymbol{w}, z)$不同；另外，树高和地形相位是PCT的两个关键输入参数，其估计误差直接影响$\hat{f}(\boldsymbol{w}, z)$的重构精度，下面分析两个因素对AGB估计模型的影响。

4.2.1 极化状态的选择对模型的影响

$\hat{f}(\boldsymbol{w}, z)$表示的是某一确定的极化状态($\boldsymbol{w}$)的相对反射率函数，在用3.1节描述的方法重构$\hat{f}(\boldsymbol{w}, z)$的过程中，如果在式(3)中计算$\tilde{\gamma}_k$时，$\tilde{\gamma}(\boldsymbol{w})$选择用相位分离最大相干优化方法获取的表面散射占主导作用的去相干$\tilde{\gamma}(\boldsymbol{w}_s)$，则得到的就是各像元的相应于表面散射占主导作用的极化状态$\boldsymbol{w}_s$的相对反射率函数，进一步提取出林分的9个特征参数，和AGB做相关性分析，

结果见表1的第2行，和体散射占主导作用的极化状态结果(表1的第1行)相比，各参数的相关系数变化不大。采用逐步回归方法选择出的3个自变量为P_4，P_7和P_8，构建的模型如表2中的模型2(M2)，和M1相比，P_4和P_8两个参数没变，P_9变成了P_7，说明在表面散射占主导作用的极化通道，$\hat{f}(\boldsymbol{w}, z)$的下半部分对生物量更敏感，而对于体散射占主导作用的极化通道，$\hat{f}(\boldsymbol{w}, z)$的上半部分更敏感，这和预期的结果一致，但是M2中，3个参数的容差很低，特别是P_7的容差仅为0.1121，说明这3个参数间存在一定程度的共线性。进一步在这3个参数间做相关性分析，发现参数P_7和P_8间的相关系数达到了0.8487；若排除参数P_7，再做多元线性回归分析，得到模型如表2中的修正模型2(MM2)，可以看到，不再存在共线性问题，回归方程显著，但和M1相比，R^2从0.9474减少到0.9287。以上分析表明，总体来看体散射占主导作用的极化状态更有利于森林AGB的估计。

4.2.2 树高反演误差对AGB模型的影响

要基于PCT算法计算$\hat{f}(\boldsymbol{w}, z)$必须首先知道每个像元的树高($\hat{h}_v$)，由PolInSAR数据直接反演$\hat{h}_v$的方法有很多，如果不考虑非体散射去相干因子($R_d$)的影响，得到的林分$\hat{h}_v$估计值与实测值的散点图见图6，平均误差为2.71 m，RMSE为4.00 m，存在高估现象。将这种方法反演的树高做为PCT的输入，重构$\hat{f}(\boldsymbol{w}, z)$，分析体散射占主导作用的极化状态的$\hat{f}(\boldsymbol{w}, z)$的9个特征参数与森林AGB的相关性，结果如表1(第3行)，各参数的相关系数略有下降。逐步回归分析的结果见表2中的模型3(M3)，P_4和P_7参数被选择为对AGB影响最显著的参数，这说明由于树高估测误差的影响，描述相对反射率函数上半部分的参数P_8和P_9对AGB的敏感性降低了，而描述结构函数下半部分的参数P_7的敏感性增强了。方程的F=71.0603，且P=0.0000，说明回归方程显著，但和M1相比，R^2从0.9474降低到0.8932。这些结果说明森林高度的估计误差会传导到$\hat{f}(\boldsymbol{w}, z)$，进而降低了基于$\hat{f}(\boldsymbol{w}, z)$估测AGB的效果。如果能联合其他的传感器，如激光雷达(LiDAR)，获得准确的树高和地形高度，就可减少树高和地形估测误差在PCT算法中的传递和累积，应该能够进一步改善$\hat{f}(\boldsymbol{w}, z)$重构的效果，进而提高AGB的估计精度。

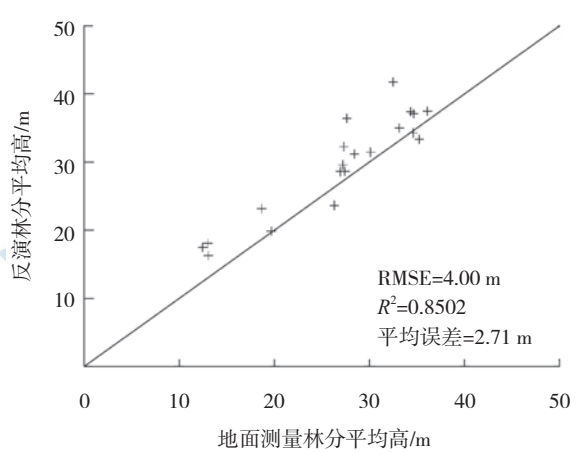

图6 基于极化相干优化的相干相位-幅度法求算的林分平均高与地面实测林分平均高的散点图，没有考虑非体去相干因子(R_d)补偿

4.2.3 与只基于林分平均高的AGB估测方法的比较

基于PolInSAR数据可以反演林分平均高，直接建立反演的林分平均高和实测林分AGB之间的回归模型也可以估测林分的AGB。用3.1节中介绍的树高估计方法得到$\hat{h}_v$后，估计各林分的林分平均高，建立如式(8)的AGB估测模型，结果如表2中的模型4(M4)，相应的散点图如图7，R^2为0.9031，RMSE=0.21 t/hm^2(自然对数值)，估计效果不如M1。

$$\ln B = -0.5270 + 1.8457 \ln(\hat{h}_m) \quad (8)$$

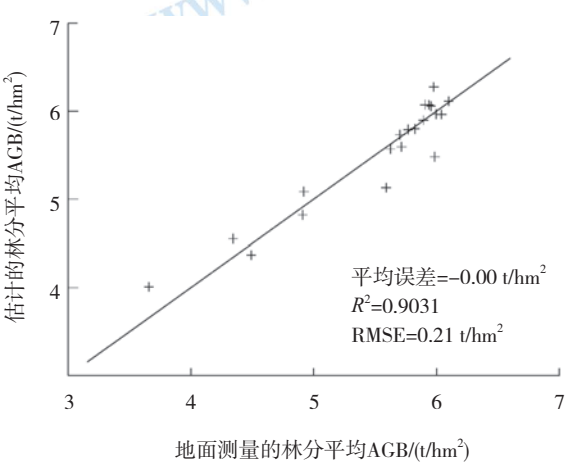

图7 基于估计的林分平均高构建回归模型，估计的林分平均AGB (自然对数)与地面实测林分平均AGB (自然对数)的散点图

对M1和M4的预测值取反函数，再和地面测量AGB做散点图分别如图8(a)(b)所示。可见，基于相对反射率函数的AGB估测模型的R^2从0.8219提高到0.8630，RMSE从57.59 t/hm^{2}减少到47.86 t/hm^2。采用10重交叉验证法比较模型1和模型4的AGB估测精度，结果显示预测AGB的平均误差从3.97 t/hm^{2}减少到0.17 t/hm^2。由此可见这3个和森林结构信息密切相关参数对AGB的解释能力大于单一林分平均高信息对AGB的解释能力，能改善AGB的估计性能。

采用M1估计的20个林分平均AGB分布图见图9(a)。图9(b)是地面测量的相应林分平均AGB分布图，由此可见，M1估测结果能很好地反应实测林分平均AGB的空间变化。

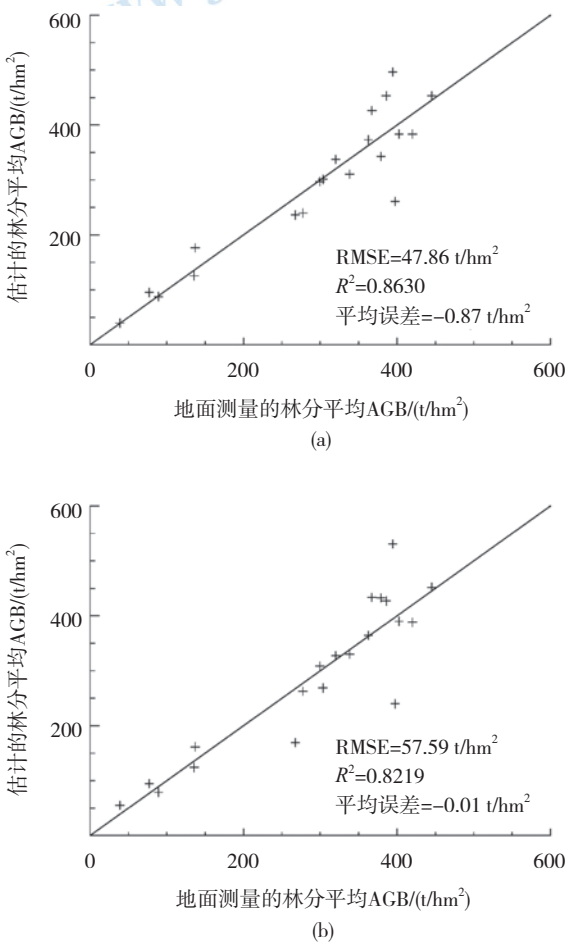

图8 回归模型估计林分平均AGB与地面实测林分平均AGB的散点图

(a) 基于提取的特征参数；(b) 只基于林分平均高

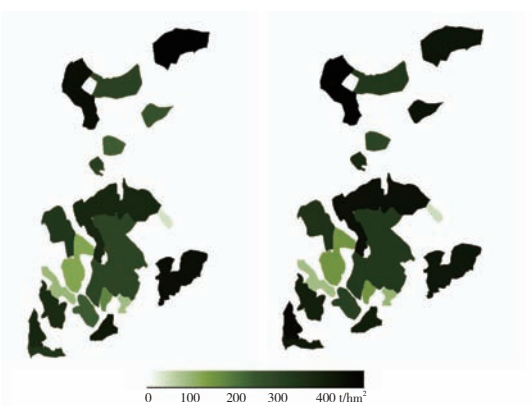

图9 林分平均AGB分布图

(a) 基于M1估计的；(b) 地面测量的

5 结 论

基于DLR机载SAR系统获取的特劳斯坦试验区L-波段PolInSAR数据，研究了使用极化相干层析技术估测森林AGB的模型和方法，通过地面样地抽样调查得到的20个林分的森林AGB数据，定量分析评价了影响本文模型和方法的AGB估测效果的主要因素，主要结论如下：

(1)通过对具有不同AGB水平的典型林分的相对反射率函数曲线的分析，定义了9个可能与AGB具有相关性的特征参数，并且与20个实测林分的AGB相关性进行分析，结果表明：除第9个参数外其他8个参数与林分平均AGB都有较好的相关性。

(2)提出了以林分平均特征参数值为自变量，以若干实测林分平均AGB为因变量，采用逐步回归分析法建立AGB估测模型的方法，分析了极化通道的选择和树高估计误差对AGB估测效果的影响，结果表明：以体散射占主导作用的极化方式的相对反射率函数建立模型要优于以表面散射占主导作用的极化方式；输入PCT的树高对AGB的估测效果有影响，树高估测误差会降低AGB的估测精度。

(3)将基于相对反射率函数特征参数的AGB估测方法与只基于林分高度的AGB估计方法进行了对比，结果表明：R^2从0.8219提高到0.8630，RMSE从57.59 t/hm^{2}减少到47.86 t/hm^2。交叉验证结果显示预测AGB的平均误差从3.97 t/hm^{2}减少到0.17 t/hm^2，表明PCT提取的相对反射率函数特征参数对AGB很敏感，充分利用相对反射率函数信息可提高AGB估计精度。

志 谢 机载极化干涉SAR数据通过中欧国际合作“龙计划”项目获取，在此对欧洲空间局表示感谢。

REFERENCES

Bai L, Cao F and Hong W. 2010. Fast approach to estimate the longest axis in coherence region and its applications. *Journal of Electronics and Information Technology*, **32**(3): 548–553 DOI: 10.3724/SP.J.1146.2009.00211

Chen E X. 1999. Development of forest biomass estimation using SAR data. *World Forestry Research*, **12**(6): 18–23

Chen X, Zhang H and Wang C. 2009. The inversion of vegetation structural parameters using dual-baseline polarimetric SAR interferometry. *Remote Sensing for Land and Resources*, **20**(4): 49–52

Cloude S R and Papathanassiou K P. 2008. Forest vertical structure

estimation using coherence tomography. IEEE International Geoscience and Remote Sensing Symposium. Boston, MA, USA: V-275-V-278

Cloude S R. 2006. Polarization coherence tomography. *Radio Science*, **41**(4): RS4017.1–RS4017.27

Cloude S R and Papathanassiou K P. 2003. Three-stage inversion process for polarimetric SAR interferometry. *IEE Proceedings-Radar, Sonarand Navigation*, **150**(3): 125–134 DOI: 10.1049/ip-rsn:20030449

Dobson M C, Ulaby F T, Pierce L E, Sharik T L, Bergen K M, Kellndorfer J, Kendra J R, Li E, Lin Y C, Nashashibi A, Sarabandi K and Siqueira P. 1995. Estimation of forest biophysical characteristics in Northern Michigan with SIR-C/X-SAR. *IEEE Transactions on Geoscience and Remote Sensing*, **33**(4): 877–895 DOI: 10.1109/36.406674

Feng Z k and Liu Y X. 2005. Precision analysis of forest biomass measuring. *Journal of Beijing Foresrry University*, **27**(S2): 108–111

Gao H X. 2005. Application of Multivariate Statistical Analysis. Beijing: Beijing University Press

Lu D S. 2006. The potential and challenge of remote sensing-based biomass estimation. *International Journal of Remote Sensing*, **27**(7): 1297–1328 DOI: 10.1080/01431160500486732

Luo H M, Chen E X, Cheng J and Li X W. 2010a. Forest height estimation methods using polarimetric SAR interferometry. *Journal of Remote Sensing*, **14**(4): 814–830

Luo H M, Li X W, Chen E X, Cheng J and Cao C X. 2010b. Analysis of forest backscattering characteristics based on polarization coherence tomography. *Science China Technological Sciences*, **53**(S1): 166–175 DOI: 10.1007/s11431-010-3242-y

Mette T. 2007. Forest Biomass Estimation from Polarimetric SAR Interferometry. Munich: Munich University of Technology

Praks J, Kugler F, Hyyppa J, Papathanassiou K and Hallikainen M. 2008. SAR coherence tomography for boreal forest with aid of laser measurements. IEEE International Geoscience and Remote Sensing Symposium, Boston: II-469-II-472 DOI: 10.1109/IGARSS.2008.4779030

Ranson K J, Sun G, Weishampei J F and Knox R G. 1997. Forest biomass from combined ecosystem and radar backscatter modeling. *Remote Sensing Environment*, **59**(1): 118–133 DOI: 10.1016/S0034-4257(96)00114-9

Steininger M K. 2000. Satellite estimation of tropical secondary forest aboveground biomass: data from Brazil and Bolivia. *International Journal of Remote Sensing*, **21**(6-7): 1139–1157

Tabb M, Orrey J, Flynn T and Carande R. 2002. Phase diversity: a decomposition for vegetation parameter estimation using polarimetric SAR interferometry. Proceedings of 4th European Synthetic Aperture Radar Conference (EUSAR 2002). Cologne

Treuhaft R N, Asner G P, Law B E and van Tuyl S. 2002. Forest leaf area density profiles from the quantitative fusion of radar and hyperspectral data. *Journal of Geophysical Research*, **107**(D21): 4568–4580

Treuhaft R N, Asner G P and Law B E. 2003. Structure-based forest biomass from fusion of radar and hyperspectral observations. *Geophysical Research Letters*, **30**(9): 1472–1475

Treuhaft R N, Chapman B D, dos Santos J R, Goncalves F G, Dutra L V, Graca P M L A and Drake J B. 2009a. The ambiguity in forest profiles and extinction estimated from multibaseline interferometric SAR. *Boletim de Ciências Geodésicas*, **15**(3): 299–312

Treuhaft R N, Chapman B D, dos Santos J R, Goncalves F G, Dutra L V, Graca P M L A and Drake J B. 2009b. Vegetation profiles in tropical forests from multibaseline interferometric synthetic aperture radar, field, and lidar measurements. *Journal of Geophysical Research*, **114**(D23): D23110.1- D23110.16

Wang C L, Guo Z X, Niu Z and Lin W P. 2006. Study on forest biophysics parameter impact on RADARSAT SAR signature. *Ecology and Environment*, **l5**(1): 115–119

Xu X J, Du H Q, Zhou G M and Fan W Y. 2008. Review on correlation analysis of independent variables in estimation models of vegetation biomass based on remote sensing. *Remote Sensing Technology and Application*, **23**(2): 239–247

Yang C J, Liu J Y, Huang H, Xu H X and Dang C L. 2005. Correlation analysis of the biomass of the tropical forest vegetation, meteorological data and topographical data. *Geographical Research*, **24**(3): 473–479

附中文参考文献

白璐，曹芳，洪文．2010．相干区域长轴的快速估计方法及其应用．电子与信息学报，**32**(3): 548–553

陈尔学．1999．合成孔径雷达森林生物量估测研究进展．世界林业研究，**12**(6): 18–23

陈曦，张红，王超．2009．极化干涉SAR反演植被垂直结构剖面研究．国土资源遥感，**20**(4): 49–52

冯仲科，刘永霞．2005．森林生物量测定精度分析．北京林业大学学报，**27**(S2): 108–111

高惠璇．2005．应用多元统计分析．北京: 北京大学出版社

罗环敏，陈尔学，程建，李小文．2010a．极化干涉SAR森林高度反演方法研究．遥感学报，**14**(4): 814–830

王臣立，郭治兴，牛铮，林文鹏．2006．热带人工林生物物理参数及生物量对RADARSAT SAR信号响应研究．生态环境，**l5**(1): 115–119

徐小军，杜华强，周国模，范文义．2008．基于遥感植被生物量估算模型自变量相关性分析综述．遥感技术与应用，**23**(2): 239–247

杨存建，刘纪远，黄河，许辉熙，党承林．2005．热带森林植被生物量与遥感地学数据之间的相关性分析．地理研究，**24**(3): 473–479